Journal of Radiation Research, 2013, 54, i147–i154
doi: 10.1093/jrr/rrt041

Study of the magnets used for a mobile isocenter carbon ion gantry

Jhonnatan Osorio MORENO*, Marco G. PULLIA, Cristiana PRIANO, Valeria LANTE, Monica M. NECCHI and Simone SAVAZZI

Centro Nazionale di Adroterapia Oncologica (CNAO), Strada Privata Campeggi, 53, Pavia, Italy
*Corresponding author. ESR-PARTNER Project WP21, Centro Nazionale di Adroterapia Oncologica (CNAO), Strada Privata Campeggi, 53, Pavia, Italy. Tel: +39-0382-078520; Fax: +39-0382-078904; Email: jhonnatan.moreno@cnao.it

(Received 21 January 2013; revised 11 March 2013; accepted 21 March 2013)

A conceptual design of a mobile isocenter carbon ion gantry was carried out in the framework of the Particle Training Network for European Radiotherapy (PARTNER) and Union of Light Ion Centres in Europe (ULICE) projects. To validate the magnets used in this gantry, Finite Element Method (FEM) simulations were performed with COMSOL multiphysics; the purpose was to evaluate the magnetic field quality and the influence of additional support structures for correctors, 90° bending dipole and quadrupoles, both in dynamic and static regimes. Due to the low ramp rates, the dynamic effects do not disturb the homogeneity and the magnetic field level. The differences between the stationary field and the corresponding dynamic field after the end of the ramps are in the order of 10^{-4}; it implies that the magnets can be operated without significant field lag at the nominal ramp rate. However, even in static regime the magnetic length of corrector magnet decreases by 5% when the rotator mechanical structure is considered. The simulations suggest an optimization phase of the correctors in the rotator.

Keywords: magnet design; magnetic length; field homogeneity; carbon ion gantry

INTRODUCTION

In carbon ion radiotherapy a rotating gantry is an attractive tool because beams can be directed to the target volume from any direction. This improvement in the dose conformation has been demonstrated by comparing the dose plan distributions that can be achieved with a gantry and with a horizontal beam line. As an example, one of the main indications for hadron therapy are tumors in the head and neck region. In particular, for a clivus chordoma, the gantry plan could achieve a reduction of up to 16% in the mean dose in the optic chiasm, which is one of the organs at risk [1]. Additional evidence for the benefits of use of gantries comes from another study performed at NIRS [2], which shows that 30% of all patients treated with a fixed line have been irradiated with couch roll angles between ±30º and ±45º for horizontal and vertical beam ports, respectively. The internal organ motion and difficult daily patient positioning problems induced by the patient rotation could be avoided by means of a gantry.

The major drawback of hadron therapy with carbon ions is the large beam rigidity, up to 6.5 T m, needed to reach deep tumors. Such a large rigidity implies large and heavy gantry structures. The only existing carbon ion gantry worldwide is located in Heidelberg (Germany) at the HIT facility. It is a fixed isocenter gantry with a radius of ~ 6.5 m and a length of 25 m. The total weight of the rotating parts in the final layout amounts to 600 tons [3].

To encourage the diffusion of carbon ion gantries, a few technical studies have been carried out, with the main purpose of reducing the size/weight and the machine cost without compromising the clinical performances. Different gantry proposals have been explored, including the use of technologies such as superconducting (SC) magnets, or the use of different ways to transport the beam, such as NS-FFAG [4]. Superconductivity offers the possibility of reducing the radius, and in particular the weight, of large bending magnets; a more compact and light gantry design therefore seems feasible. However, even if the technology of rotating an SC magnet was available, a lot of development would be necessary for it to be used in a gantry. The main challenges are AC losses, temperature margins of superconducting materials, rotation of the cooling system, fringing fields and difficulties in designing the mechanical structure for holding the magnetic forces [5]. NS-FFAG technology allows for the reduction of the gantry weight, but this concept requires the scanning

magnets to be downstream of the last bending, which implies large gantry size [4]. A recent study carried out within the framework of the PARTNER-WP21 and ULICE-WP6 European projects, suggests a solution based on normal conducting magnets and on the concept of a mobile isocenter gantry, whereby the patient is displaced, instead of moving the whole beam line around the patient [6]. In the proposed mobile isocenter gantry, the patient is inside a mobile cabin, as shown in Fig. 1. The isocenter position is then defined with respect to the patient cabin rather than to a fixed room. Normal conducting magnet technology has been chosen because it is well established and current experience guarantees the feasibility of the magnet design.

Active beam delivery systems (scanning magnets) are usually recommended nowadays for carbon ion systems, because the fragmentation generated by passive systems generates an undesirable dose increment in the skin and in the organs at risk. The large impact on the gantry geometry is due to the position of the scanning magnets with respect to the last dipole. If the scanning magnets are placed downstream of the last bending dipole, the distance between the isocenter and the magnet has to be large in order to accommodate the Source to Axis Distance (SAD), and a significant skin dose contribution (approximately 20% due to divergent scanning) is estimated in order to keep the gantry radius to reasonable size [5]. If the scanning magnets are placed upstream of the 90° dipole, parallel scanning can be obtained with a proper choice of the pole face angles of the bending magnet. Parallel scanning is very appealing since it corresponds to infinite SAD and a negligible increase in skin dose [5]. For the previous reasons, upstream scanning has been chosen for the gantry design.

The main advantages of this layout are the reduction in the number of magnetic elements, a shorter gantry length, a reduction of the gantry weight, and a reasonably consistent economical saving [5, 6]. This article outlines the key results of using finite element magnets simulations (FEMs) to validate the conventional warm magnets to be included in the final gantry layout.

MATERIALS AND METHODS

The design of conventional accelerator magnets is often driven by the integrated field quality (ΔBL/BL) in the region traversed by the beam, the Good Field Region (GFR), the main factor to be considered in the design of the magnets. It influences the size of the magnet gap and the pole shape, and consequently the quantity of iron to be used in the magnet. Figure 2 and Table 1 show the layout of the magnets and the main technical specifications of three types of magnets included in the gantry: quadrupoles, correctors and the final 90° bending dipole, respectively.

Modeling considerations

The software used for the calculations was COMSOL multiphysics [7], which solves the field equations with boundary conditions by finite element discretization. The general COMSOL approach to solving electromagnetic problems is to use the vector potential description in all the geometries that define the magnet model. Every iron magnet yoke was modeled as non-linear material, considering its own BH curve. Quadrupole and corrector coils were modeled as racetrack type, and the 90° bending magnet coils were modeled as curved bedstead type. Additionally, the coil water

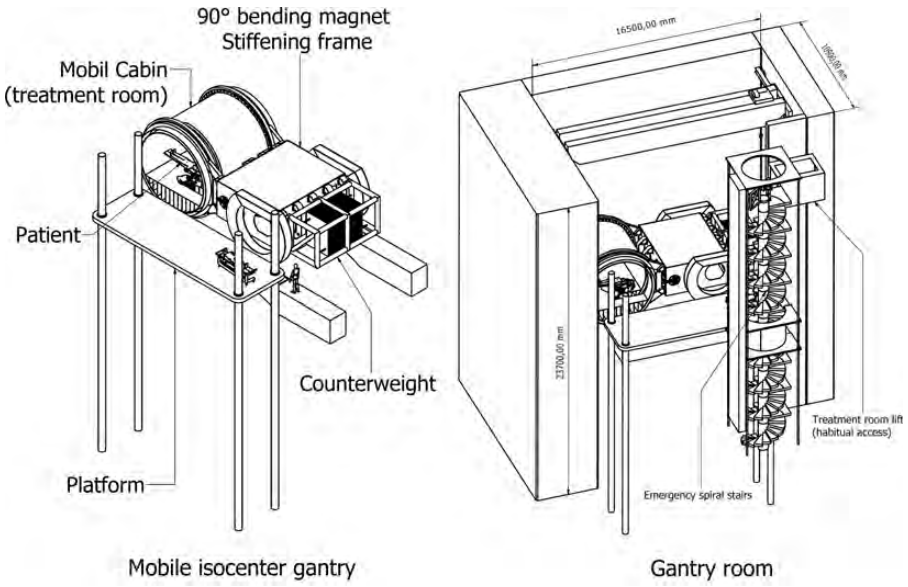

Fig. 1. Mobile isocenter gantry layout.

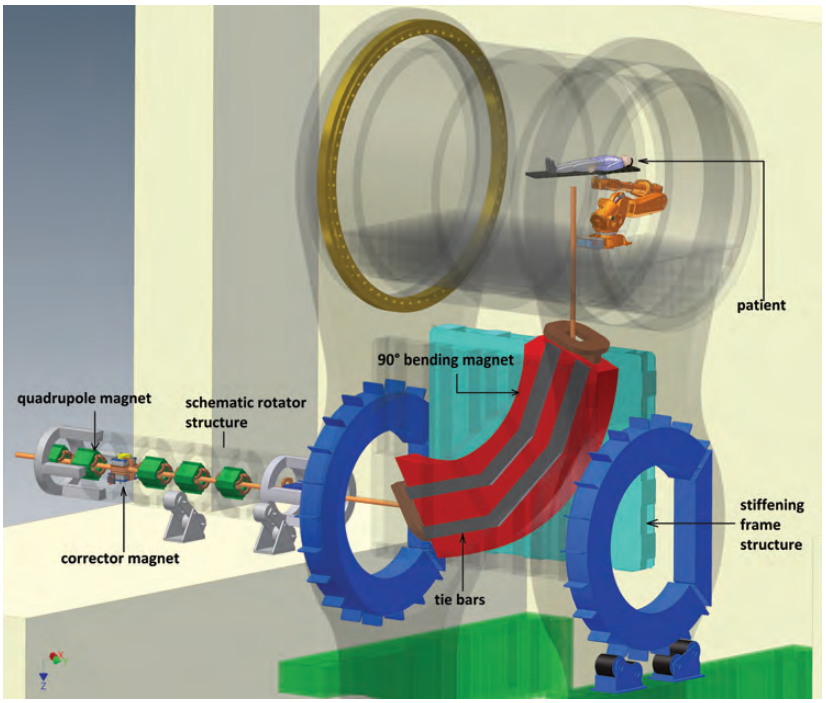

Fig. 2. Schematic layout of the magnets used in the mobile isocenter gantry.

Table 1. Main functional specifications requested in the gantry layout and some additional information concerning the holding mechanical structure

Parameter	90° bending dipole	Corrector dipole	Quadrupole magnet
Nominal field (T) or gradient field (T/m)	1.81	0.06	18
Ramp rate (A/s) (sigmoid curve shape)	506.6	280	572.5
Good Field Region (GFR) (mm × mm)	±100 × ±100	±30 × ±30	radius = 30 mm
Nominal current (A)	2280	140	286
Number of turns per pole	80	40	70
Maximum temperature coil raise (°C)	20	13	20
Integrated field quality (ΔBL/BL) or gradient (ΔGL/GL)	$\leq \pm 2 \times 10^{-4}$	$\leq \pm 1 \times 10^{-2}$	$\leq \pm 1 \times 10^{-3}$
Magnetic length (mm)	5734	520	450
Type of iron yoke material	EBG 1200-100A	EBG STABOCOR M 270-35A	EBG 1200-100A
Number of tie bars	24	0	4
Type of surrounding ferromagnetic structure	Stiffening frame	Rotator structure	Rotator Structure

temperature rise was kept below 20 °C; Table 1 shows the particular coil details. The models were built using tetrahedral meshes in the regions of low interest, like the external air, and hexahedral meshes were used in the interesting regions (iron yoke and GFRs) where the mean mesh size was 2.5 mm; finer tetrahedral meshes were used to connect the GFR, coils and yoke.

Quadrupoles and correctors were modeled both outside and inside their rotating support structure. In this way the influence of the mechanical structure on their magnetic field was evaluated both in dynamic and in static regimes. Compared with the other magnets, the final 90° dipole is a very large device with a very large gap. Due to the need for placing the scanning magnets in upstream configuration, the final bending magnet needs to have a large aperture, at least equal to the treatment field. This magnet provides magnetic fields up to 1.81 T in a GFR of 20×20 cm^2 and it is ~ 6 m long with a weight of ~ 100 t. Its yoke is subdivided into six parts, which are assembled to form the complete magnet. It requires an external mechanical structure to provide the

necessary stiffness. The stiffening structure was also modeled and considered in the FEM calculations. In the 2D simulations reported in this article, the reference system was placed such that the center of symmetry of every magnet corresponded to the origin of the reference system (apart from the 90° bending magnet which was modeled in axial symmetry [7]). The vertical axis corresponded to the y coordinate, and the horizontal (radial) axis corresponded to the $x(r)$ coordinate. The definition of field quality for the 2D (equations 1 and 2) and magnetic length for the 3D simulations (equation 3) are:

$$\frac{\Delta B}{B} = \left(\frac{\|B(x,y) - B(0,0)\|}{\|B(0,0)\|}\right)_{dipole} \quad (1)$$

$$Q_g = \frac{\Delta B}{B_0} = \frac{\sqrt{\left(\sum_{n=6,10...}^{\infty} \beta_{n_r} \sin(n\theta)\right)^2 + \left(\sum_{n=6,10...}^{\infty} \beta_{n_\theta} \cos(n\theta)\right)^2}}{\beta_2} \quad (2)$$

$$\text{where} \begin{cases} \beta_{n_r} = \frac{1}{\pi}\int_0^{2\pi} B_r \sin(n\theta) d\theta B_r = \sum_{n=2,6,10..}^{\infty} \beta_{n_r} \sin(n\theta) \\ \beta_{n_\theta} = \frac{1}{\pi}\int_0^{2\pi} B_\theta \cos(n\theta) d\theta B_\theta = \sum_{n=2,6,10..}^{\infty} \beta_{n_\theta} \cos(n\theta) \end{cases}$$

$$L = \frac{\int_{\text{beam path}} |B(x,y,z)dl|}{|B(0,0,0)|} \text{ magnetic field length} \quad (3)$$

Equation 2 describes the field quality in terms of multipole expansion of the field for the quadrupole magnet case. In this case it was evaluated for the limit of the GFR, (i.e. at a circumference centered at (0,0) with radius $r = 30$ mm). Eddy currents are generally an undesired effect, and are generated during the excitation current ramp phase. To minimize eddy currents, the iron yoke was laminated; however, some structural elements, like the tie bars welded externally to the magnet, are non-laminated, which could give rise to detrimental effects. Two-dimensional dynamic studies were performed in order to evaluate the effect on the field quality and to calculate the time delay induced by these additional ferromagnetic elements.

RESULTS

90° bending dipole simulation results

Two-dimensional static simulation results of the 90° bending magnet are shown in Fig. 3; a nominal current of 2280 A was used. The influence of the stiffening frame and the tie bars on the magnetic field quality in the center of the magnet is shown in Fig. 4.

The influence of different structures on the magnetic field intensity was estimated by evaluation of the magnetic field in the center point of the GFR. The tie bars and the stiffening frame have an influence on the field intensity in the GFR. This is more evident in the case of the tie bars, which cause an increment of about 0.82% of the magnetic field strength in the gap, while the contribution of the stiffening frame is smaller and accounts for a variation of 0.1%. Further details of static simulations are reported in Table 2.

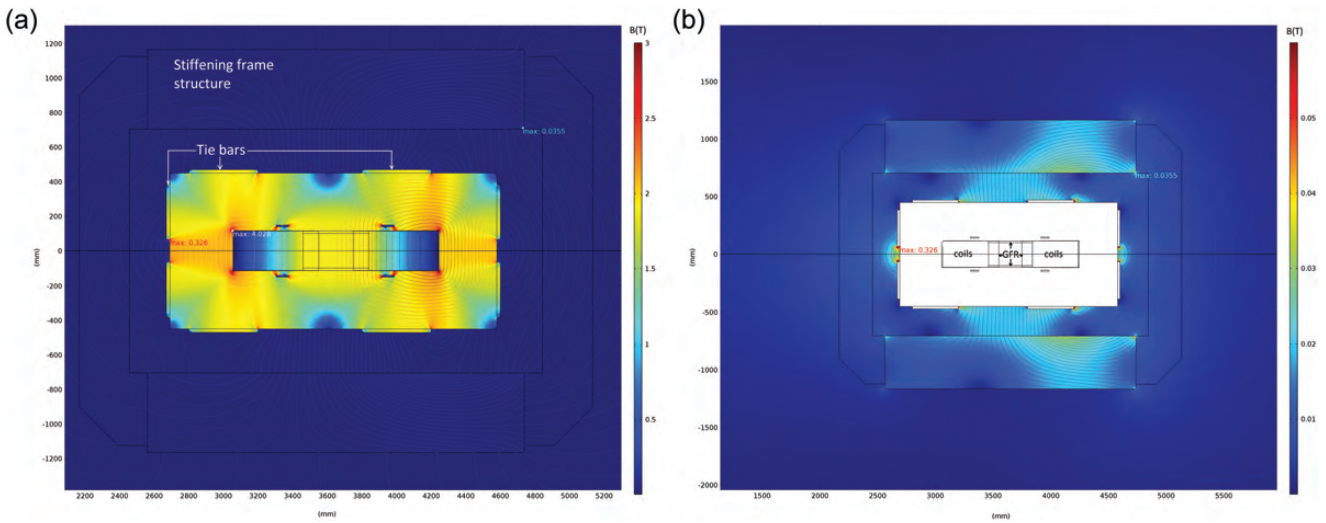

Fig. 3. **a**) Magnetic flux density of the 90° bending magnet. **b**) Magnetic flux density detail on stiffening frame and external air. Maximum field values are sorted by colors: white = iron yoke, red = air, blue = stiffening frame. Horizontal and vertical axes correspond to the physical dimensions of the magnet.

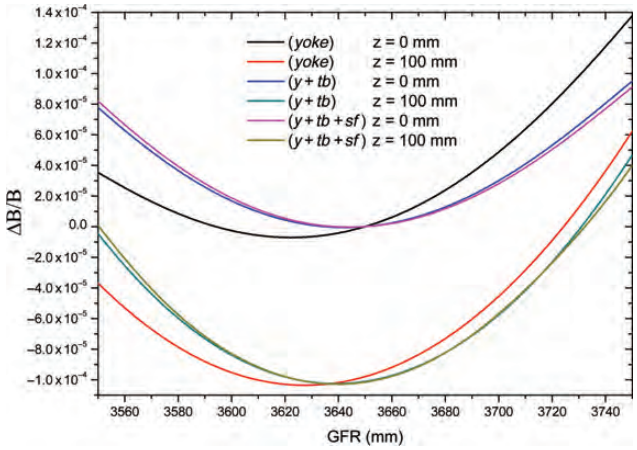

Fig. 4. Effect of tie bars and stiffening frame on the field quality of the 90° bending magnet. *yoke* = iron yoke, *tb* = tie bars, *sf* = stiffening frame. The abscissa scale corresponds to the GFR length in Fig. 3.

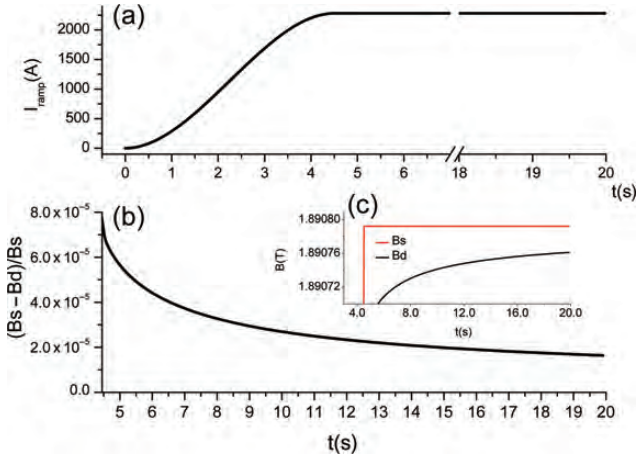

Fig. 5. Dynamic simulation of the 90° bending magnet considering tie bars and stiffening frame structure. **a**) Feeding current ramp up to I_{max} = 2280 A (t_{ramp} = 4.5 s) and dI/dt = 506.6 A/s. **b**) Relative differences between static (Bs) and dynamic fields (Bd) at the end of the ramp. **c**) detail of the magnetic field intensities after the end of the ramp.

Table 2. Summary of the 2D static and dynamic simulations of the 90° bending magnet

Magnetic field in the gap (T)	**1.89**
$\Delta B/B_0$ at GFR	$(-1.03 \times 10^{-4}, 1.41 \times 10^{-4})$
Stored Energy (J)	1 213 924.48
Inductance (H)	0.47
Dissipated DC power (kW)	613.65
DC voltage (V)	269.16
Exponential time constant of the lagging part of the field (s)	1.13

Figure 4 shows the magnetic field homogeneity along lines in the center and at the vertical limit of the GFR. The quantity shown is ΔB/B for three different cases: "*yoke*", which represents the FEM calculation considering only the iron yoke structure, "*y* + *tb*", representing the calculation including the tie bars and "*y* + *tb* + *sf*", which includes all the structures involved. In all cases the magnetic field homogeneity was always better than $\pm 10^{-4}$ in the entire GFR.

Dynamic simulations

The effects induced by the eddy currents on the central field were estimated by the magnetic field intensity evaluation in the center of the GFR. Figure 5 shows the difference between the dynamic field simulation (Bd) and the field calculated in static conditions (Bs). The initial time, 4.5 s, corresponds to the end of the current ramp.

As shown in Figure 5, the amount of field lagging at the end of the ramp, (Bs-Bd)/Bs, is $<10^{-4}$. Moreover only a small variation in field is made when changing energy and all the time needed for acceleration is available for settling. Altogether no visible effect was expected on the beam. A summary of the main characteristics calculated for the 90° bending magnet is reported in Table 2.

Quadrupole and corrector simulations

Quadrupole

The technical specifications of the extraction line quadrupoles have been shown in Table 1. These quadrupoles are laminated and tie bars are used to keep laminations together. Figure 6 shows the gradient field homogeneity evaluated by equation 2 at the limit of the GFR of the 2D FEM quadrupole simulation (i.e. r = 30 mm and $0° \le \theta \le 45°$).

The field gradient calculated at the nominal current was 19.481 T/m, which is in excess of the specified 18 T/m. The effect of the rotator structure was negligible, and only 0.11% of gradient increment was given by the tie bars. The calculated field quality fulfilled the specifications considering tie bars and rotator frame (Figure 6).

Dynamic simulations were also carried out for quadrupoles (Figure 7). The time constant was 0.93 s, mainly due to the tie bars and not to the rotator structure. As for the dipole, the size of the lagging field was small and the design was considered suitable for the intended operation.

Corrector magnet

The corrector has no tie bars, thus only the effect on the field generated by the rotator mechanical structure was studied. Figure 8 shows the field induced on the rotator structure by the corrector magnet.

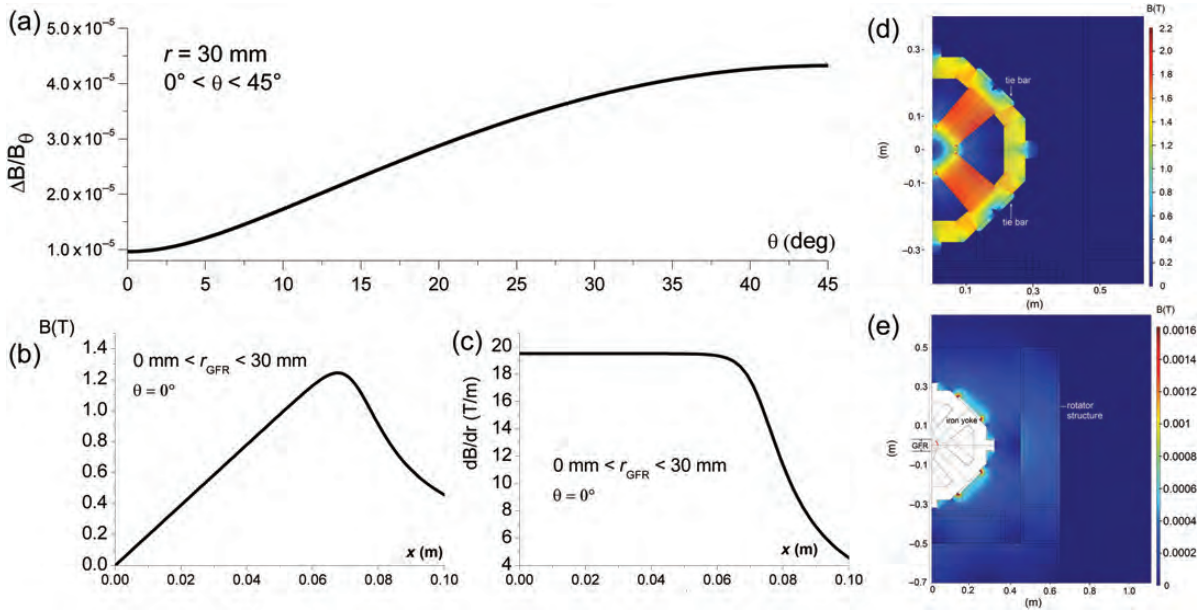

Fig. 6. Main simulated characteristics of quadrupole magnet in static regime and considering tie bars and rotator structure. **a**) Gradient field quality calculated using equation 2. **b**) Magnetic field. **c**) Field gradient. **d**) Magnetic flux density. **e**) Magnetic flux density detail on air and rotator structure. Feeding current used was I = 286 A.

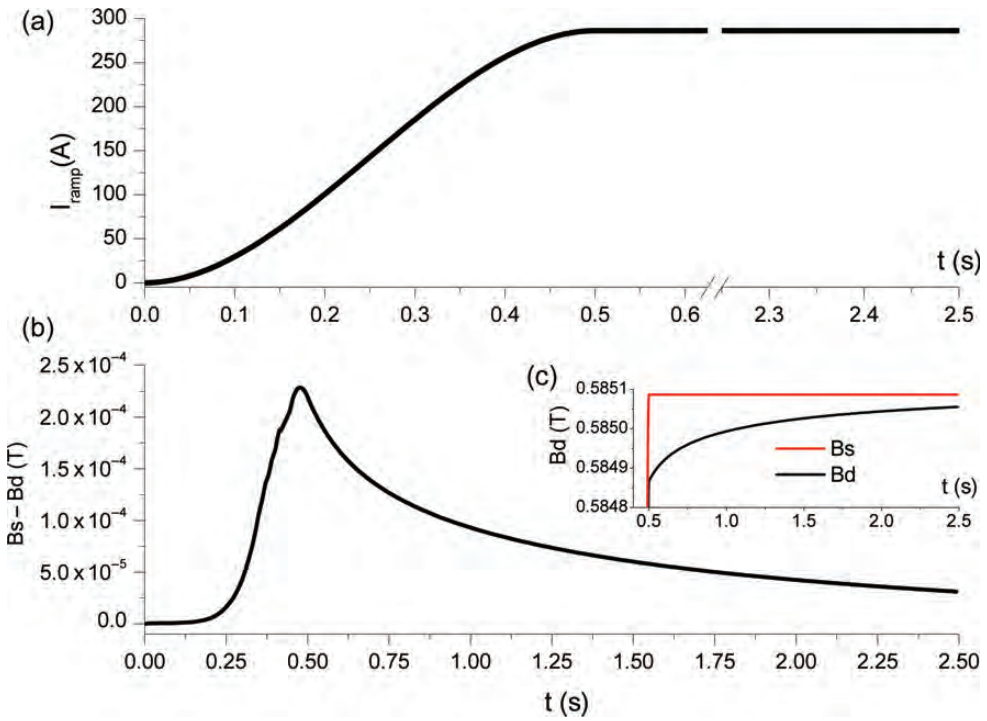

Fig. 7. Dynamic simulation of quadrupole magnet evaluated in the boundary of the GFR (r = 30 mm; θ = 0°) modeled for tie bars and rotator structure. **a**) Feeding current ramp up to I_{max} = 286 A (t_{ramp} = 0.5 s) and dI/dt = 572.5 A/s. **b**) Differences between static (Bs) and dynamic (Bd) during the ramp period. **c**) Detail of the magnetic field intensities after the end of the ramp.

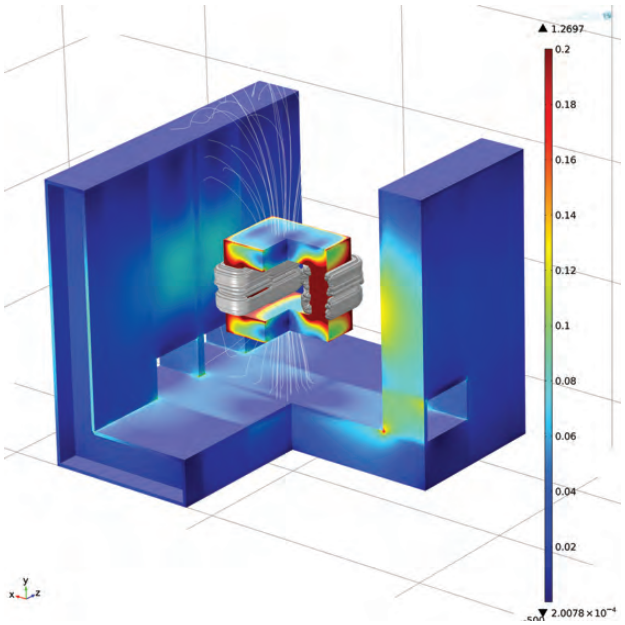

Fig. 8. 3D FEM corrector + rotator model. A quarter of the geometry has been cut to show the magnetic field induced inside the rotator.

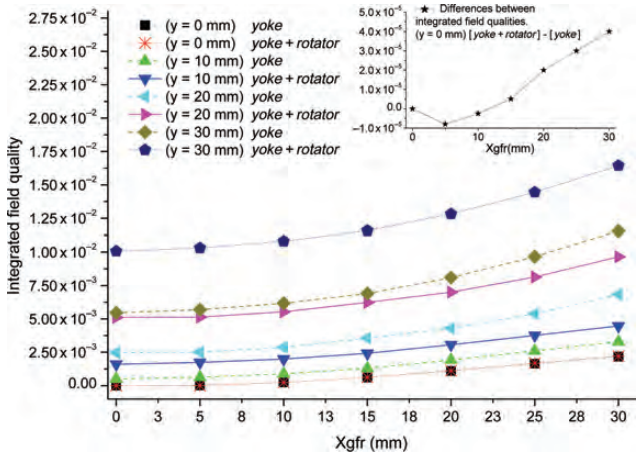

Fig. 9. Integrated field quality of the corrector magnet in different horizontal positions of the GFR. Upper right, detail of the difference between integrated field qualities of *yoke* and *yoke* + *rotator* at *y*=0 mm.

It is worth noting that there is a significant field level in the rotator, which is due to the fact that the corrector coils are not shielded by the yoke, creating a non-null dispersed field beside the magnet. The magnetic length (proportional to the integrated field) and the integrated field homogeneity are shown in Figures 9 and 10. As is evident, the rotator structure had a large effect on the magnetic length, changing it from 535.23 to 508.49 mm, which represents a length reduction of 5%. Apart from a few percent variation in the absolute value,

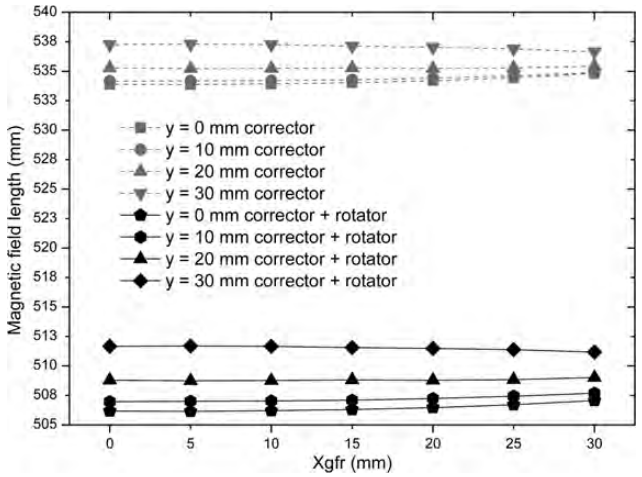

Fig. 10. Magnetic field length calculated in different horizontal positions (Xgfr) in the GFR.

the ΔB/B value was almost doubled when the mechanical structure was considered in the simulation (Figure 9).

A summary of the main results for the quadrupole and corrector magnets calculations are reported in Table 3. The dynamic behavior of the corrector was simulated as well, but the absence of tie bars made the time constant much shorter than in the previous cases and the field lag was negligible.

DISCUSSION

The main magnets used in the gantry design were simulated with FEM codes. Both static and dynamic simulations were made, showing that eddy currents in the solid iron around the laminated magnet have a visible influence on the magnetic field in the GFR. The decay constant of the eddy currents can be relatively long, in the order of 1 s, but the amount of field that is lagging sufficiently small to have an acceptable variation on the beam, considering that the magnet is ramped when the beam is not yet in the gantry beam line. As an example, the characteristics of the CNAO synchrotron can be considered [8]. The beam time needed for a irradiating a patient is determined by the number of spills requested for a specific treatment plan. Typically, the nominal number of spills for a treatment session is about 60 and each of them lasts ~ 1 s, and the nominal session time is ~ 3 min. When the tumor slice changes (i.e. the tumor depth and, consequently, the beam energy change), the synchrotron magnets are washed in order to be ready to accelerate the new beam with the new requested energy. In this phase, the extraction line does not need to wash its magnets since it only has to adjust the field for the slight energy difference between the previous beam and the new beam.

In the case presented in this study, corresponding to the 90° bending magnet, the washing cycle was performed just

Table 3. Summary of main results simulated for the quadrupole and corrector magnets, considering all the surrounding structures

	Corrector	Corrector + rotator	Quadrupole	Quadrupole + rotator
Field or Gradient Intensity	6.06×10^{-2} T	6.06×10^{-2} T	19.48 T/m	19.50 T/m
Field or gradient homogeneity	$\leq 1.15 \times 10^{-2}$	$\leq 1.64 \times 10^{-2}$	$\leq 1.0 \times 10^{-3}$	$\leq 1.0 \times 10^{-3}$
Exponential time constant of the lagging part of the field (s)	0.07	0.07	0.93	0.93
Magnetic length (mm)	535.23[a]	508.49 [a]	461.75 at $(r, \phi) = (30$ mm, $45°)$	461.75 at $(r, \phi) = (30$ mm, $45°)$

[a]Average value.

once, with the consequence that the energy variations for the different tumor slices were accomplished by means of small current changes, guaranteeing the same path for the magnet hysteresis curve. We concluded that the lagging field was much less than 10^{-4} and could be disregarded, since the washing cycle was performed just once for a treatment field.

The effect of the mechanical structure of the rotator was particularly strong for the orbit corrector magnets; in this case, the resulting homogeneity was almost acceptable, but an optimization of the design of the correctors in the rotator could be considered. In absolute terms, a reduction of the field integral > 5% can easily be compensated with a slightly higher excitation current.

FUNDING

This work was supported by the European Community in the Seventh Framework Program, 2007–2012 PARTNER Project (Grant Agreement no. 215840-2).

REFERENCES

1. Jäkel O, Debus J. Selection of beam angles for radiotherapy of skull base tumors using charged particles. *Phys Med Biol* 2000;**45**:1229–41.
2. Noda K. Rotating gantry for HIMAC facility. 2nd Workshop on Hadron Therapy of Cancer, Erice, 2 3rd May, 2011. http://erice2011.na.infn.it/TalkContributions/Noda-23.pdf (8 March 2013, date last accessed).
3. Heidelberg Ion-Beam Therapy Center. http://www.klinikum.uni-heidelberg.de/Facts-Figures.129368.0.html?&L=1 (12 December 2012, date last accessed).
4. Trbojevic D, Morozov V. Innovative superconducting non scaling fixed field alternating gradient isocentric gantry for carbon cancer therapy. Proceedings of IPAC 2011, San Sebastián, Spain. *WEPS029*:p2544–46. http://accelconf.web.cern.ch/accelconf/IPAC2011/papers/weps029.pdf (8 March 2013, date last accessed).
5. Lante V, Necchi MM, Savazzi S *et al*. Deliverable Report JRA 6.3. Conceptual design of a carbon ion gantry. ULICE, 2007–2013. 126 pp. https://espace.cern.ch/ULICE-results/Shared%20Documents/Deliverable%20JRA%20WP6-3_public.pdf (8 March 2013, date last accessed).
6. CERN. Proton-ion medical machine study (PIMMS) Part I. CERN/PS 99-010 (DI), Geneva, 1999. 223 pp. http://cdsweb.cern.ch/record/385378/files/ps-99-010.pdf (12 December 2012, date last accessed).
7. COMSOL multiphysics, http://www.comsol.com/ (8 March 2013, date last accessed).
8. Rossi S. *et al*. The status of CNAO. *Eur Phys J Plus* 2011;**126**:78. http://www.cnao.it/documents/2011/EurPhysJPlus2011-126-78.pdf (8 March 2013, date last accessed).